NINTH EUROPEAN ROTORCRAFT FORUM

Paper No. 53

PARAMETRIC TIP EFFECTS FOR CONFORMABLE ROTOR APPLICATIONS

WAYNE R. MANTAY

NASA/Langley Research Center
Army Structures Laboratory
Hampton, Virginia
U.S.A.

WILLIAM T. YEAGER, JR.

NASA/Langley Research Center
Army Structures Laboratory
Hampton, Virginia
U.S.A.

September 13-15, 1983

STRESA, ITALY

Associazione Industrie Aerospaziali

Associazione Italiana di Aeronautica ed Astronautica

PARAMETRIC TIP EFFECTS FOR CONFORMABLE ROTOR APPLICATIONS

ABSTRACT

This research study was initiated to systematically determine the impact of selected blade tip geometric parameters on aeroelastically conformable rotor performance and loads characteristics. The model articulated rotors included baseline and torsionally soft blades with interchangeable tips. Seven blade tip designs were evaluated on the baseline rotor and three tip designs were tested on the torsionally soft blades. The designs incorporated a systematic variation in three geometric parameters: sweep, taper, and anhedral. The rotors were evaluated in the NASA Langley Transonic Dynamics Tunnel at several advance ratios, lift and propulsive force values, and tip Mach numbers. Based on the test results, tip parameter variations generated significant rotor performance and loads differences for both baseline and torsionally soft blades. Azimuthal variation of elastic twist generated by the tip parameters strongly correlated with rotor performance and loads, but the magnitude of advancing blade elastic twist did not.

1.0 Introduction

Reducing helicopter vibratory loads while improving performance through passive control has been the goal of the Aeroelastically Conformable Rotor (ACR) concept. Initial ACR studies (ref. 1) examined the potential of a conformable rotor to alter the unfavorable blade spanwise and azimuthal load distributions which lead to increased vibratory bending loads and power requirements. In reference 1, test results on a model hingeless rotor indicated that elastic twist measurably changed blade loads on a torsionally soft blade. Promising methods of achieving this passive control concept, incorporating time varying elastic twist, have been identified analytically (ref. 2), and blade design features producing that desired elastic control were sought for an articulated rotor.

The effect of blade tip shape on rotor performance and loads has received much attention for application to multibladed helicopters (refs. 3-5). Experimental data have also been obtained (ref. 6) which initiated identification of the blade tip shape as a promising passive control concept. The reference 6 test utilized a model rotor blade with conventional torsional stiffness. Although the resulting loads and performance of the configurations were tip-shape-dependent, the identification of which parameter caused each load or performance change was elusive. This was due, in part, to multiple parameter variations occurring with each tip change. Nevertheless, the concept of passive control to achieve better rotor

performance while reducing loads was encouraged by these results and several conformable designs were pursued. The resulting studies (refs. 7-8) considered variations in blade torsional stiffness, airfoil section, mass distribution, and trailing edge tab deflection, as well as tip geometry, in the design. Again, the wind-tunnel tests of these ACR concepts produced encouraging loads and performance data, but the aeroelastic mechanism for design success or failure was not obvious.

Expanded testing and analysis of the configurations of reference 6 resulted in identification of several key issues for future ACR application and development (ref. 9). For the torsionally stiff rotor used in that test, the parametric variations of tip sweep, taper and anhedral did measurably change the elastic twist and integrated performance, but there did not appear to be a strong connection between elastic twist and performance. Additional tests on the blades of ref. 8 which incorporated large tip spans and trailing edge tab deflections (refs. 10-11) showed performance and loads variations which, though significant, were not easily explainable by individual parameter effects.

The parameters most effective in improving conformable rotor performance and loads characteristics have thus not been systematically determined. Although it has been shown that changes in adjustable trailing edge tabs have significant effects on conformable rotor behavior (ref. 11), the rotor blade tip operates in a very influential portion of the rotor disk and thus provides significant research impetus. This is especially true if ACR success is dependent on elastic twist control. Consequently, the research study described herein was initiated to systematically determine the impact of selected blade tip geometric parameters on ACR performance and loads characteristics.

2.0 Notation

a speed of sound, ft/sec

b blade number

C_D rotor drag coefficient, $\frac{D}{\rho\pi R^2(\Omega R)^2}$

C_L rotor lift coefficient, $\frac{L}{\rho\pi R^2(\Omega R)^2}$

$\overline{C_L}$ nominal rotor lift coefficient

C_Q rotor torque coefficient, $\frac{Q}{\rho\pi R^3(\Omega R)^2}$

c	blade chord, in.
c.g.	section measured center of gravity location, in.
a.c.	section computed aerodynamic center location, in.
D	rotor drag, lb.
H	longitudinal rotor force perpendicular to control axis, lb.
L	rotor lift, lb.
M_T	rotor blade tip Mach number, $\frac{\Omega R}{a}$
Q	rotor torque, ft-lb.
r	blade radial station, ft
R	rotor radius, ft
V	free-stream velocity, ft/sec
α_s	angle of attack of rotor shaft, deg.
$\Delta\theta_1$	elastic twist angle, positive nose-up, deg.
μ	rotor advance ratio, $\frac{V}{\Omega R}$
ρ	mass density of test medium, slug/ft^3
σ	nominal rotor solidity ratio, $bc/\pi R = .082$
σ_A	rotor area solidity ratio, $\frac{\text{total blade area}}{\text{rotor disk area}}$
ψ	azimuth angle of rotor blade, deg
Ω	rotor rotational speed, rad/sec
ω	natural frequency of rotating blade, rad/sec

2.1 Abbreviations

R	rectangular
S	swept
T	tapered
A	anhedral

3.0 Apparatus

3.1 Wind Tunnel

The experimental program was conducted in the Langley Transonic Dynamics Tunnel (TDT) shown in figure 1. The TDT is a continuous flow tunnel with a slotted test section. The tunnel test section is 16 ft square with cropped corners and has a cross-sectional area of 248 ft^2. Freon-12[1] was used as the test medium in the TDT for this program. Because of its high density and low speed of sound, the use of Freon-12 aided the attempt to match full-scale Reynolds number while achieving full-scale Mach number values. Also, some restrictions on model structural design are eased, while dynamic similarity is still maintained. The heavier test medium permits a heavier structural design to obtain the required stiffness characteristics and thus eases the design and fabrication requirements of the model (refs. 12, 13). For this investigation, Freon-12 at a nominal density of .006 $slug/ft^3$ was used as the test medium.

3.2 Model Description

All the experimental blades described herein were tested on the Aeroelastic Rotor Experimental System (ARES) shown in figures 2 and 3. The ARES has a generalized helicopter fuselage shape enclosing the rotor controls and drive system. It is powered by a variable frequency synchronous motor connected to the rotor shaft through a belt-driven two-stage speed reduction system. The ARES rotor control system and pitch attitude (α_s) are remotely controlled from within the wind-tunnel control room. The ARES pitch attitude is varied by an electrically controlled hydraulic actuator. Blade collective pitch and lateral and longitudinal cyclic pitch are input to the rotor through a conventional swashplate. The swashplate is moved by three hydraulic actuators.

3.3 Description of Rotor Blades

The rotor models used in this investigation were 0.175-scale, four-bladed articulated rotors with coincident lead-lag and flapping hinges. The blade geometry was the same for both baseline and soft torsional rotors tested and is shown in figure 4. The blades were designed so that the tip configuration could be changed at the 89 percent radius. The

---

[1]Freon: Registered trademark of E.I. du Pont de Nemours & Co., Inc.

baseline swept tip blades approximately represented a current full-scale utility-class rotor system in planform. An SC1095 airfoil was used on all blades from the root cutout to 49 percent radius and from 91 percent radius to the tip. Between 50 and 90 percent radius, a cambered SC1095-R8 airfoil was used. A smooth transition was provided between the different airfoil sections. Adjustable trailing edge tabs of 6.5 percent chord exist on both baseline and ACR blades; the tab setting was 0° for this test.

The baseline blades were aeroelastically scaled, but blade dynamic characteristics did not precisely represent any specific full-scale rotor. The ACR blades differed from the baseline only in torsional stiffness over the outer 55 percent of the blade span. The blade physical properties are the same as the blades of reference 10 and the natural frequencies are presented in Table I.

3.4 Instrumentation

Instrumentation on the ARES allows continuous displays of model control settings, rotor forces and moments, blade loads, and pitch link loads. ARES pitch attitude is measured by an accelerometer, and rotor control positions are measured by linear potentiometers connected to the swashplate. Rotor blade flapping and lagging are measured by rotary potentiometers mounted on the rotor hub and geared to the blade cuff. Rotor shaft speed is determined by a magnetic sensor. One blade of each blade set, baseline and ACR, was instrumented with four-arm strain-gage bridges to measure loads and deflections at four blade radial stations. Flapwise (out-of-plane) moments and chordwise (in-plane) moments were measured at 26, 39, 53, and 81 percent radius, while torsional moments were measured at 29, 37, 52, and 78 percent radius. The rotating blade data are transferred through a 30-channel slip-ring assembly. Rotor forces and moments are measured by a six-component strain-gage balance mounted below the pylon and drive system. The balance is fixed with respect to the rotor shaft and pitches with the fuselage. Fuselage forces and moments are not sensed by the balance.

3.5 Description of Parametric Tips

Seven blade tip designs were evaluated on the baseline rotor and three of these tip designs were tested on the torsionally soft blades. The tip designs incorporated a systemmatic variation in three geometric parameters: sweep, taper, and anhedral. These parameters were varied while all tips had the same target values of inertial properties, airfoil contour, and twist. The magnitude of the sweep angle and taper ratio chosen for ACR application were representative of

current design values for modern helicopter rotors. The magnitude chosen for tip anhedral is typical of previous investigations. Figure 5 presents the geometry of the tip designs, while Table II lists the measured tip characteristics and compares them to the design targets. Airfoil section tolerances were held to ±.002 in. The value of σ used throughout this report for normalizing performance coefficients is 0.082, based on a blade nominal chord of 3.6 inches and a radius of 56.2 inches. Table II also gives the values of weighted solidities.

4.0 Test Methodology

The test procedure was designed to facilitate comparison between tip configurations. Each rotor configuration was first tracked and balanced in hover in the Freon test medium to remove first harmonic fixed system loads. At each forward flight test point, the rotor rotational speed and tunnel conditions were adjusted to give the desired tip Mach number and advance ratio, at the desired shaft angle of attack. Blade collective pitch was changed to obtain the target rotor lift and propulsive force; and at each collective pitch setting, the cyclic pitch was used to remove rotor first-harmonic flapping with respect to the rotor shaft. Data were then recorded at each value of rotor task. The maximum rotor task attained at each shaft angle of attack was determined in most cases by either blade load limits or ARES drive system limits. Aerodynamic rotor hub tares were determined with the blades removed throughout the ranges of shaft angle of attack and advance ratio investigated. Both deadweight and hub aerodynamic tares have been removed from the data presented herein.

4.2 Accuracies

Based on replicated data points, the repeatability of the data for constant shaft angle of attack, control angles and advance ratio has been estimated to be within the following limits:

$$\frac{C_L}{\sigma} \pm 0.0025$$

$$\frac{C_D}{\sigma} \pm 0.0004$$

$$\frac{C_Q}{\sigma} \pm 0.00015$$

The accuracy for angle measurements is estimated to be within ±0.25°.

4.3 Test Conditions

All the tip configurations shown in Figure 5 were tested on the baseline stiffness blade for the target conditions shown in Table III. The magnitudes of lift and propulsive force parameters, tip Mach number, and advance ratio were chosen as representative of a modern utility helicopter. The ACR low torsional stiffness blades were used to test three tips for the target conditions of Table III. These tips were chosen because of their interesting performance and loads characteristics when tested on the baseline blades, as will be described later in this paper. The ACR tip planforms are those of Figure 5c, f, and g: swept, swept anhedral, and swept tapered anhedral. Within the scope of this paper, the performance and loads data presented for analysis emphasizes the target lift and shaft angle combinations of Table III, at one rotational tip Mach number (0.65), and two advance ratios (0.35, 0.40).

5.0 Results

5.1 Rotor Performance

Fixed system forces and torque were obtained using the procedures and limits described earlier for all tip configurations and conditions of Table III. Parametric performance results for selected conditions are presented in Figure 6. The advance ratios and lift coefficients were selected for presentation because they showed the most significant difference in rotor performance between configurations.

The effect of tip shape on baseline rotor performance for the complete set of tips is shown in Figure 7. Each vertical vector represents the percent reduction in torque coefficient for a given rotor task for each tip shape. Each horizontal vector serves to label the added parameter for each tip. This method of presentation of rotor performance allows the separation of parametric geometry effects to be easily visualized. For the baseline blades tested and the conditions shown, the rotor's performance was enhanced by the addition of anhedral to a rectangular planform and the addition of sweep to the tapered planform. Tip taper alone enhanced rectangular rotor performance at $\mu = .35$ conditions but not at higher speeds ($\mu = .40$). The independent effect of torsional stiffness is not included in Figure 7.

The tip configurations which were tested on the torsionally soft blade were chosen because of the good performance these tips gave the baseline blade. As shown in figure 6 however, these configurations exhibited higher torque requirements than their baseline counterparts for the same rotor tasks.

5.2 Rotor Loads

Blade oscillatory loads are important not only from vibratory and fatigue considerations but also because they provide insight into blade loading environment and elastic deformation trends. Torsional loads and flapwise oscillatory loads are associated with local blade loading and twist (ref. 8). Figure 8 presents 1/2 peak-to-peak flapwise loads at four spanwise stations for all configurations tested. These oscillatory loads are data points taken at the μ, M_{TIP}, C_L/σ and α_s values listed for each tip configuration. The configurations are also ranked in Figure 8 according to their performance at the C_D/σ values shown. The rank of 1 is the lowest torque required for the rotor task. Examination of figure 8 shows a significant relationship between performance and oscillatory flapwise loads. Specifically, the configurations which exhibited the lowest flapwise loads were also the best performers with regard to C_Q/σ while the poor performance configurations generated the highest flapwise loads.

5.3 Elastic Twist

Spanwise distributions of blade torsional moment time histories were converted to elastic twist distributions through known torsional stiffness properties of the blade, control system, and UH-60 model hub. This is shown in Figure 9 for all configurations tested at the μ, M_{TIP}, C_L/σ and α_s values listed. Some interpolation of the inboard torsional loads was occasionally necessary. Figure 9 indicates the elastic twist is configuration-dependent for each rotor task and, as might be expected, varies with rotor environment. Note the compressed vertical scale for the ACR configurations. The elastic twist waveforms are comprised of several harmonics, but are dominated by the one per rev torsional moments.

The amount of azimuthal activity in the elastic twist plots is significant when compared with the integrated rotor performance for each configuration. Elastic twist activity is noted by the number and magnitude of waveform peaks around the azimuth. Figure 9 waveforms have been ordered according to each configuration's torque coefficient for the rotor tasks shown with the lowest torque configuration appearing first, and the highest torque configuration last in each case. A correlation between rotor performance and elastic twist is evident in the data shown. Specifically, the configurations which exhibited small azimuthal activity in elastic twist were the best performers.

6.0 Analysis of Results

The performance and loads data for the baseline and ACR configurations were examined to provide insight into the mechanism by which the tip planform and torsional stiffness parameters affected the aeroelastic environment of the rotor blades. The controlled differences between configurations were evaluated for the fundamental changes they caused in the rotor's performance and response in light of past and current conformable design concepts.

6.1 Rotor Performance Analysis

Several of the tip shape configurations, namely those incorporating taper, possessed slightly less area solidity than the untapered tips. This alone might be expected to produce performance differences which may be significant, depending on the rotor task involved. Additionally, several configurations utilized anhedral in the tip area, which can project a different area to the airstream than the comparable straight blade. In order to isolate and quantify these inelastic effects, a rigid blade performance analysis was utilized.

Rotor performance characteristics and azimuthal distributions of rotor-blade-section angle of attack were calculated with a computer program using a strip-theory implementation of the equations presented in reference 14. In the analysis, the blade was assumed to be rigid with pitch and flap degrees of freedom but no lag degree of freedom. The rotor airfoil section characteristics used were obtained from reference 15. Changes in section aerodynamic coefficients with angle of attack and Mach number were included in the analysis. All calculations were made by using both a uniform inflow model and the nonuniform inflow model from reference 16. Reference 16 considers a rotor load distribution which closely resembles that of a typical rotor and yields a non-iterative solution for the induced velocity at any point on the rotor. The validity of this model was largely confirmed by reference 17.

For selected rotor task conditions, Figure 10 shows predicted performance changes due to solidity and anhedral, for both uniform and non-uniform inflow models. The effect of taper alone on rotor performance trends is predicted by both inflow models, although the magnitude of each configuration's torque coefficient is fairly well predicted only by the non-uniform inflow model. The effect of tip anhedral on rotor performance trends and torque magnitude is not well predicted by this rigid blade analysis for either inflow model. Because this analysis does not incorporate a vortex wake even for its non-uniform inflow model, and because anhedral is expected to modify the location of tip vortices in the wake (ref. 6), it is

not surprising that tip anhedral effects cannot be adequately modeled. The inability of a rigid blade analysis to totally account for performance changes due to tip solidity variations has been noted previously, for example, in reference 9. It should be noted that past efforts in correlating model-scale and full-scale rotor performance have been less than successful when blade dynamics was not adequately modeled (ref. 18). Therefore, inclusion of blade dynamics effects in predicting performance is thought to be important for most rotor planforms.

6.2 Blade Elastic Twist Magnitude

Past aeroelastically conformable rotor design concepts have considered the magnitude of advancing blade elastic twist as a solution to a potentially unfavorable angle of attack environment (ref. 2, for example). Depending on the tip airfoil section and advancing blade Mach number, a nose-up elastic twist was thought to be desirable on the advancing side to achieve lower rotor torque and blade loads. Figure 11 presents elastic twist magnitudes on the advancing side ($\psi = 90°$) for each configuration and rotor task shown. Figure 11 also contains the total geometric pitch angle (which is comprised of elastic twist, built-in twist, collective and cyclic pitch angles) at $\psi = 90°$. Both types of blade angle data are also ranked according to their configuration's performance, with number 1 requiring the least torque for a given rotor task.

As is evident from Figure 11, there is no strong correlation between the magnitude of each configuration's advancing blade elastic or total pitch angle and the performance of the rotor. It is recognized that configuration performance and loads depend on local angle of attack which is affected by inflow distribution as well as pitch angle and that non-uniform inflow velocity can be very sensitive to planform configuration. Nevertheless, aeroelastically conformable rotors have been designed to achieve specific azimuthal placement of elastic twist magnitudes and the present study does not support the effectiveness of this design goal.

6.3 Conformable Rotor Control

Conformable rotors which effect significant blade torsional response may generate rotor control characteristics which should be evaluated for their contributions to rotor stability and control (ref. 8). Throughout the test program described herein, all configurations were easily controlled through the model actuator-swashplate system for all test conditions. The amount of control needed to achieve each rotor task was configuration-dependent. Figure 12 shows, for a representative rotor task, the longitudinal cyclic pitch

required to remove first harmonic flapping with respect to the rotor shaft for several configurations which differ in blade torsional stiffness. The differences in elastic twist measured for these configurations, also included in Figure 12, is offset by control input differences of nearly the same magnitude in order to remove the first harmonic flapping with respect to the rotor shaft. The differences in longitudinal cyclic pitch for these configurations is significant not so much for control travel considerations, but for what these angles reveal about the rotor behavior for these tips and torsional stiffnesses.

An interesting phenomenon was observed in both the pitch control required to trim the rotor and the rotor task achieved, in particular, the rotor propulsive force. For a given advance ratio, tip Mach number, force normal to the trimmed tip path plane, and shaft angle of attack, the torsionally soft rotor configurations consistently exhibit less propulsive force. This can be seen in the performance data of Figure 6. Resolution of the rotor balance forces reveals that this decrease in rotor propulsive force occurs for two primary reasons. First, the control axis for the torsionally soft rotor has tilted aft due to the changes in longitudinal pitch mentioned above. Secondly, the rotor longitudinal force perpendicular to the control axis (H-force) is greater for the torsionally soft blade while the thrust was maintained constant. The control axis aft tilt is due to the rotor control used in the test and the nose-down elastic twist magnitude observed. The H-force increase for the ACR configurations is probably due to an increase in integrated drag loading on the advancing side of the azimuth. This drag increase would also manifest itself in decreased rotor efficiency, a fact which was shown earlier in this paper for these configurations.

6.4 Blade Loading

It is well known that the radial and azimuthal distribution of rotor blade loading can affect both performance and loads. The potential of the conformable rotor concept to tailor these airloads has, in fact, been viewed as a key to the optimization of rotor performance (ref. 2). Specifically, a redistribution of airloads which avoids sharp radial and azimuthal gradients in loading has been investigated for rotor performance improvement (ref. 19).

As previously shown, the rotor configurations described in this paper which exhibited good performance and low vibratory loads generated the least activity in elastic twist around the azimuth. Since several configurations provided significant aerodynamic center-elastic axis offsets, the elastic twist variations observed may be primarily due to oscillatory tip lift. Although section pitching moment variations may add to elastic twist perturbations around the azimuth, these would also be lift dependent.

It is therefore possible that the success of those configurations which exhibited low vibratory loads and increased performance is based on a redistribution of lift either radially or azimuthally, or both. The clue to the apparent airload redistribution may be found in the parameter combinations which aeroelastically complement each other. For example, as has been shown previously in figure 7, anhedral seems to aeroelastically help a rectangular tip planform more than it does a swept-tapered planform. Furthermore, the addition of sweep seems to enhance the aerodynamic environment of a tapered planform more than it does a rectangular tip for the configurations tested.

These examples illustrate the complex relationship between tip geometry and blade aeroelastic environment which may be largely responsible for determining rotor performance. The beneficial parameter couplings may, for example, alleviate compressible effects and adverse loadings on a rotor blade via 3-D aerodynamics or angle of attack adjustments. In any case, the reduction in tip loading gradients is manifested in the elastic twist activity and results in good rotor performance. The use of an aeroelastic analysis would be necessary to qualify this observation, but the test results included herein support the hypothesis that both performance improvements and load reductions are generated by the same aeroelastic mechanism.

7.0 Conclusions

Based on the data obtained, and for the test conditions and model configurations investigated, the following conclusions have been reached:

1. Significant performance and loads differences were generated among the seven tip parameter variations.

2. Torsionally soft rotor (ACR) applications for the tip shapes tested resulted in poorer performance and usually higher loads than for the baseline configuration.

3. The configurations which exhibited the lowest oscillatory flapwise loads also had the best performance while the configurations with poor performance generated the highest flapwise loads.

4. There does not exist a strong correlation of advancing blade elastic twist magnitude with rotor performance and flapwise loads.

5. There exists a strong correlation between azimuthal variation of elastic twist and rotor performance and loads. The configurations which exhibited small azimuthal activity in elastic twist were the best performers.

9.0 References

1. Doman, Glidden S.; Tarzanin, Frank J.; and Shaw, John, Jr.: Investigation of Aeroelastically Adaptive Rotor Systems. Proceedings of a Symposium on Rotor Technology, American Helicopter Society, August 1976.

2. Blackwell, R. H.; and Merkley, D. J.: The Aeroelastically Conformable Rotor Concept. Preprint No. 78-59, 34th Annual Forum Proceedings, American Helicopter Society, May 1978.

3. Berry, John D.; and Mineck, Raymond E.: Wind-Tunnel Test of an Articulated Helicopter Rotor Model With Several Tip Shapes. NASA TM 80080, 1980.

4. Stroub, Robert H.; Rabbott, John P., Jr.; and Niebanck, Charles F.: Rotor Blade Tip Shape Effects on Performance and Loads From Full-Scale Wind Tunnel Testing. Journal of the American Helicopter Society, Volume 24, No. 5, October 1979, pp. 28-35.

5. Philippe, J. J.; and Vuillet, A.: Aerodynamic Design of Advanced Rotors with New Tip Shapes. 39th Annual Forum Proceedings, American Helicopter Society, May 1983, pp. 58-71.

6. Weller, William H.: Experimental Investigation of Effects of Blade Tip Geometry on Loads and Performance for an Articulated Rotor System. NASA TP 1303, 1979.

7. Sutton, Lawrence R.; White, Richard P., Jr.; and Marker, Robert L.: Wind-Tunnel Evaluation of an Aeroelastically Conformable Rotor. USAAVRADCOM TR-81-D-43, 1982.

8. Blackwell, R. H.; Murrill, R. J.; Yeager, W. T., Jr.; and Mirick, P. H.: Wind Tunnel Evaluation of Aeroelastically Conformable Rotors. Preprint No. 80-23, 36th Annual Forum Proceedings, American Helicopter Society, May 1980.

9. Yeager, William T., Jr.; and Mantay, Wayne R.: Wind-Tunnel Investigation of the Effects of Blade Tip Geometry on the Interaction of Torsional Loads and Performance for an Articulated Helicopter Rotor. NASA TP 1926, 1981.

10. Yeager, William T., Jr.; and Mantay, Wayne R.: Loads and Performance Data From a Wind-Tunnel Test of Model Articulated Helicopter Rotors With Two Different Blade Torsional Stiffnesses. NASA TM 84573, 1983.

11. Blackwell, R. H.; and Fredrickson, K. C.: Wind-Tunnel Evaluation of Aeroelastically Conformable Rotors. USAAVRADCOM TR-80-D-32, 1981.

12. Lee, Charles: Weight Considerations in Dynamically Similar Model Rotor Design. SAWE Paper No. 659, May 1968.

13. Hunt, G. K.: Similarity Requirements for Aeroelastic Models of Helicopter Rotors. C.P. 1245, Royal Aircraft Establishment, 1973.

14. Gessow, Alfred; and Crim, Almer D.: A Method for Studying the Transient Blade-Flapping Behavior of Lifting Rotors at Extreme Operating Conditions. NACA TN 3366, 1955.

15. Noonan, Kevin W.; and Bingham, Gene J.: Aerodynamic Characteristics of Three Helicopter Rotor Airfoil Sections at Reynolds Numbers From Model Scale to Full Scale at Mach Numbers From 0.35 to 0.90. NASA TP-1701, AVRADCOM TR 80-B-5, 1980.

16. Mangler, K. W.; and Squire, H. B.: The Induced Velocity Field of a Rotor. R. & M. No. 2642, British A.R.C., May 1950.

17. Heyson, Harry H.; and Katzoff, S.: Induced Velocities Near a Lifting Rotor With Nonuniform Disk Loading. NACA Rep. 1319, 1957. (Supersedes NACA TN 3690 by Heyson and Katzoff and TN 3691 by Heyson.)

18. Yeager, William T., Jr.; and Mantay, Wayne R.: Correlation of Full-Scale Helicopter Rotor Performance in Air With Model-Scale Freon Data. NASA TN D-8323, 1976.

19. Moffitt, Robert C.; and Bissell, John R.: Theory and Application of Optimum Airloads to Rotors in Hover and Forward Flight. 39th Annual Forum Proceedings, American Helicopter Society, May 1982.

Table I. Model Rotor Blade Rotating Natural Frequencies at Ω = 68.07 rad/sec

Baseline ω/Ω	Mode Identity	ACR ω/Ω
2.68	Flapwise	2.65
	Torsion	4.48
4.98	Flapwise	4.93
5.08	Chordwise	4.98
7.06	Torsion	
8.17	Flapwise	8.17

Table II. Model Rotor Blade Tip Characteristics

Design Target	Tip c.g. location (in.)		Tip weight (grms)	Tip twist (deg)	c.g.-a.c. / c (pos. c.g. forward)		
	Chordwise 1.236	Spanwise 2.774	71	1.35	.96R	.98R	1.0R
Tip Configuration							
Rectangular	1.30	2.75	73.1	1.27	.028	-.05	.02
Tapered	1.24	2.82	73.4	1.27	-.014	-.056	.007
Swept	1.50	2.85	73.6	1.27	.096	-.04	.019
Swept Tapered	1.31	2.94	71.4	1.27	.096	-.017	.008
Rectangular Anhedral	1.31	2.75	71.1	1.14	.028	-.05	.02
Swept Anhedral	1.48	2.96	70.4	.93	.096	-.04	.019
Swept Tapered Anhedral	1.25	3.00	71.8	1.27	.096	-.017	.008

Rotor Solidity

	Tapered Configurations	Non-tapered Configurations
Area solidity	.08127	.08252
Thrust-weighted solidity	.07905	.08263
Torque weighted solidity	.07793	.08259

Table III. Target Test Conditions

μ	M_{TIP}	α_s	$\frac{C_L}{\sigma}$	α_s	$\frac{C_L}{\sigma}$	α_s	$\frac{C_L}{\sigma}$
.30	.65 .68 .70	-6.0°,-7.8°	.06	-4.5°,-5.9°	.08	-3.6°,-4.7°	.10
.35	.65 .67	-8.2°,-10.5°	.06	-6.1°,-7.9°	.08	-4.9°,-6.3°	.10
.40	.63 .65	-10.6°,-13.6°	.06	-8.0°,-10.3°	.08	-6.4°,-8.3°	.10

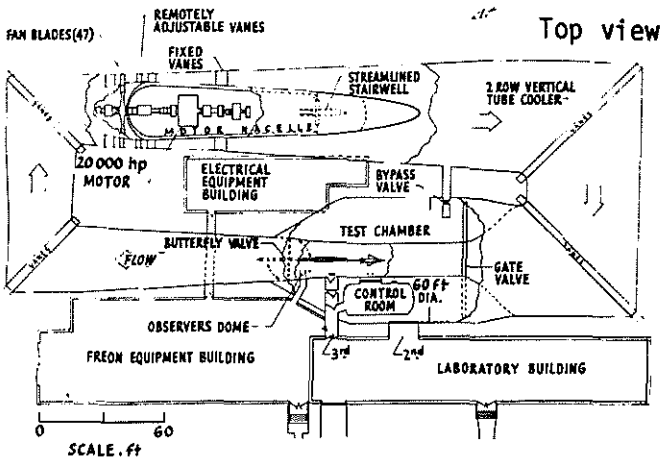

Figure 1.- Langley Transonic Dynamics Tunnel.

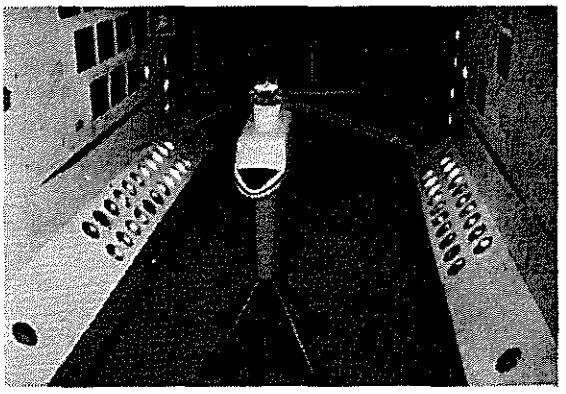

Figure 2.- Aeroelastic rotor experimental system (ARES) model in Langley Transonic Dynamics Tunnel.

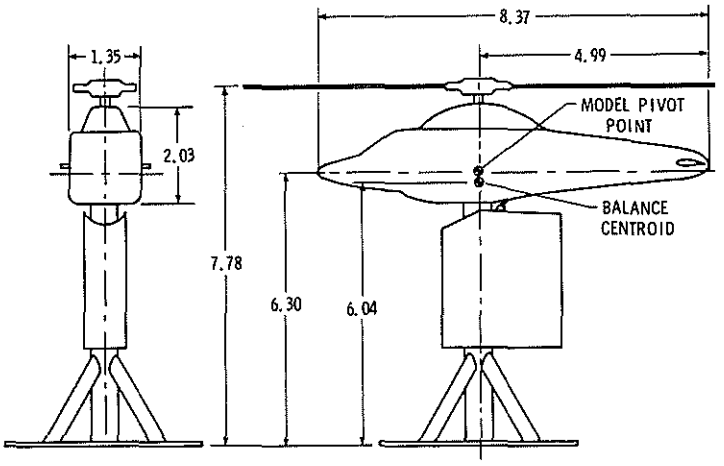

Figure 3.- Schematic diagram of aeroelastic rotor experimental system. All dimensions are in feet.

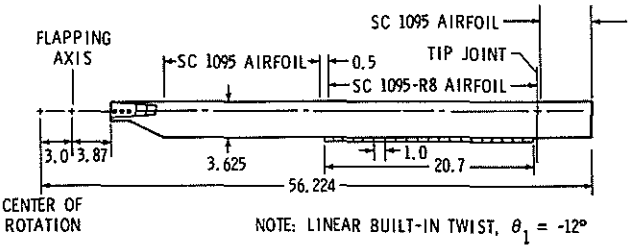

Figure 4.- Rotor blade geometry. Blade dimensions are in inches.

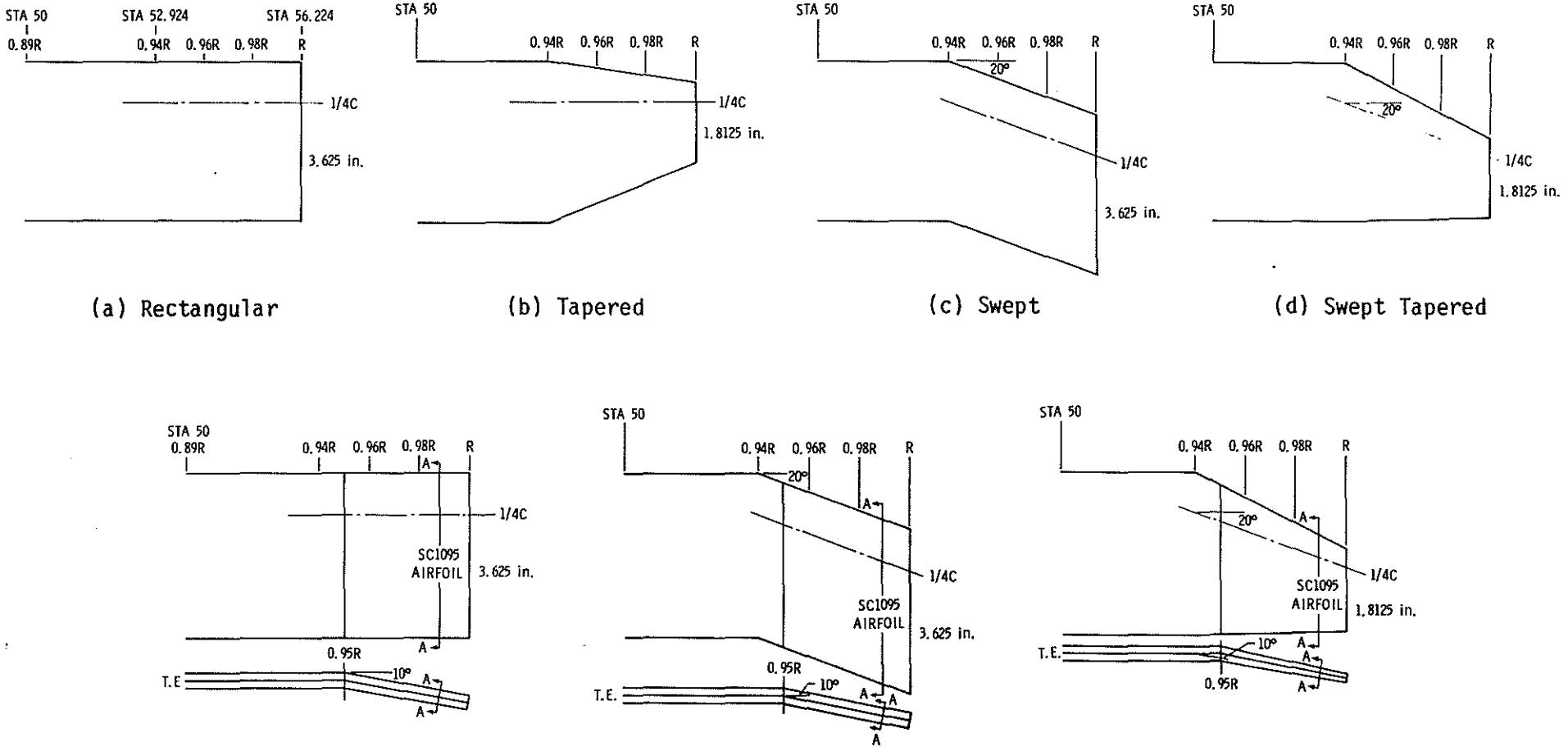

(a) Rectangular (b) Tapered (c) Swept (d) Swept Tapered

(e) Rectangular Anhedral (f) Swept Anhedral (g) Swept Tapered Anhedral

Figure 5.- Geometry of tips tested. Dimensions are in inches unless otherwise indicated.

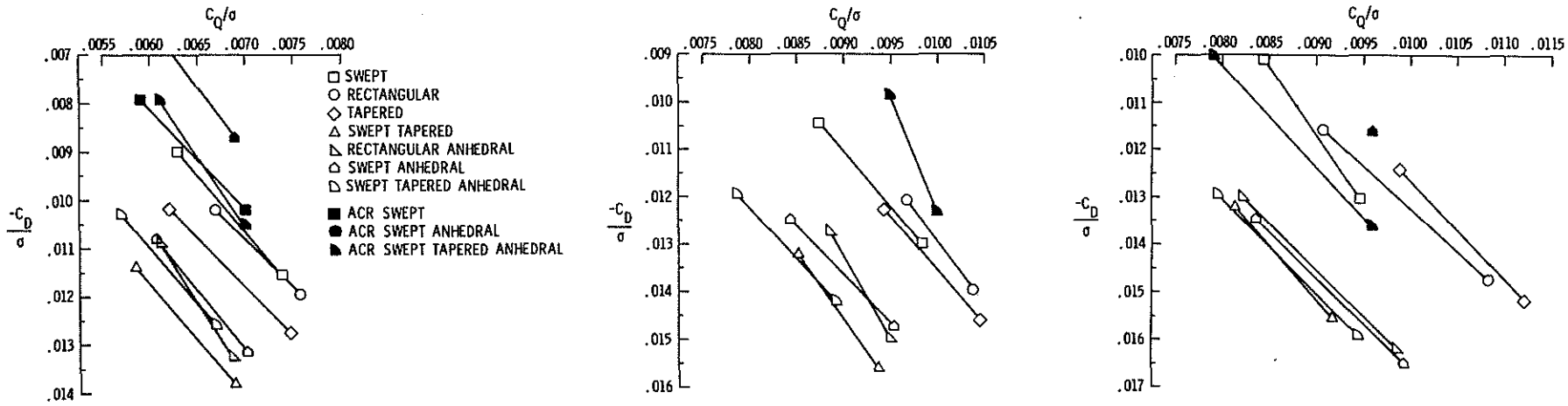

(a)
$\mu = .35$
$M_{TIP} = .65$
$\frac{C_L}{\sigma} = .07872$

(b)
$\mu = .35$
$M_{TIP} = .65$
$\frac{C_L}{\sigma} = .098$

(c)
$\mu = .40$
$M_{TIP} = .65$
$\frac{C_L}{\sigma} = .07885$

Figure 6.- Experimental rotor performance.

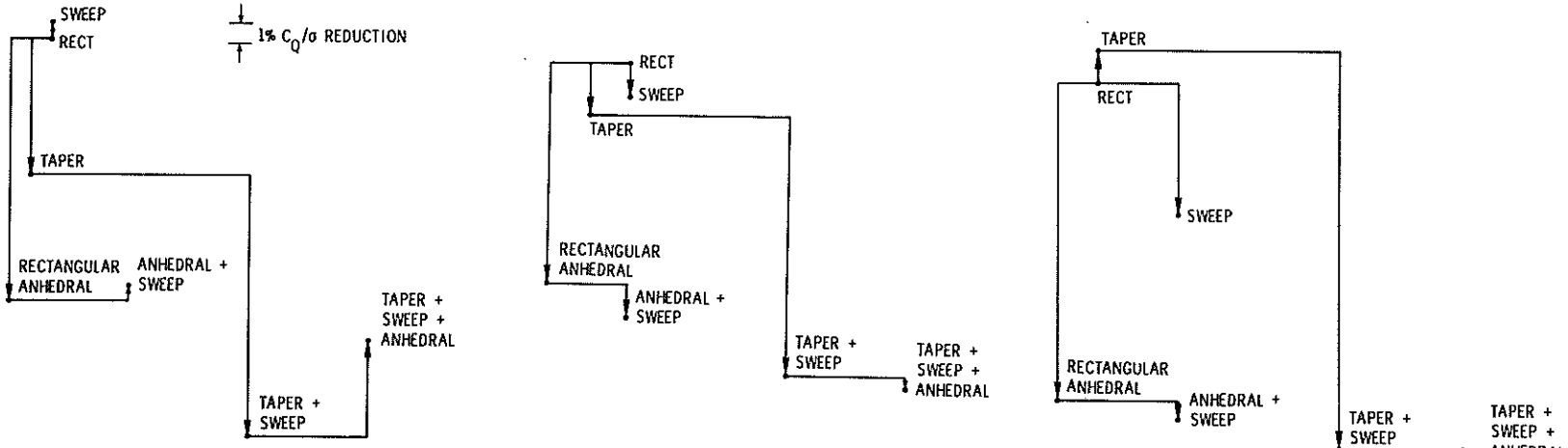

(a)

$\mu = .35$

$M_T = .65$

$\frac{\bar{C}_L}{\sigma} = .07872$

$\frac{C_D}{\sigma} = -.0110$

(b)

$\mu = .35$

$M_T = .65$

$\frac{\bar{C}_L}{\sigma} = .098$

$\frac{C_D}{\sigma} = -.01325$

(c)

$\mu = .40$

$M_T = .65$

$\frac{\bar{C}_L}{\sigma} = .07885$

$\frac{C_D}{\sigma} = -.0145$

Figure 7.- Parametric tip shape effect on experimental baseline rotor performance.

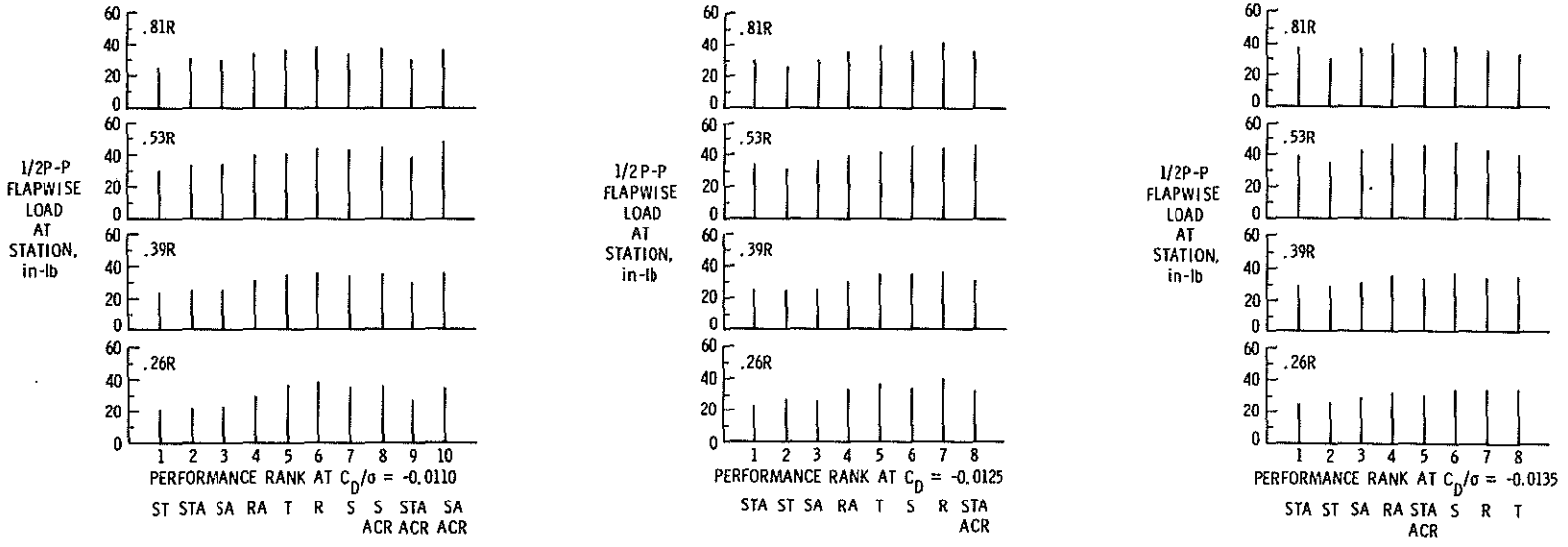

(a)

μ = .35

M_T = .65

$\frac{\overline{C}_L}{\sigma}$ = .07872

σ_s = -6.1°

(b)

μ = .35

M_T = .65

$\frac{\overline{C}_L}{\sigma}$ = .098

σ_s = -4.9°

(c)

μ = .40

M_T = .65

$\frac{\overline{C}_L}{\sigma}$ = .07885

σ_s = -8.0°

Figure 8.- Flapwise oscillatory blade loads versus rotor performance.

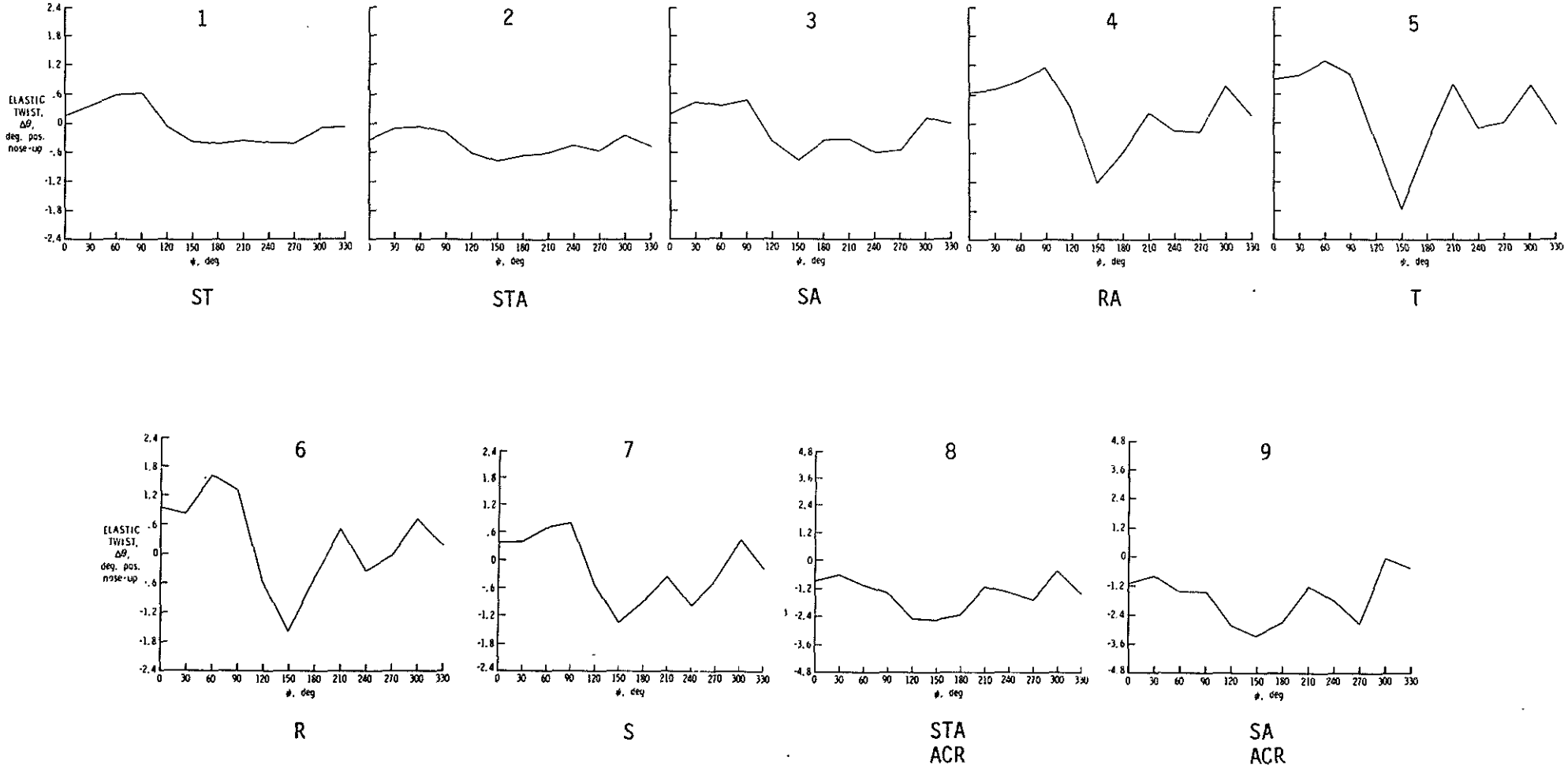

(a) $\mu = .35$ $M_T = .65$ $\frac{\overline{C}_L}{\sigma} = .07872$ $\alpha_s = -6.1°$. Performance rank at $C_D/\sigma = -.0110$

Figure 9.- Radial distribution of elastic twist versus azimuth at .78 R.

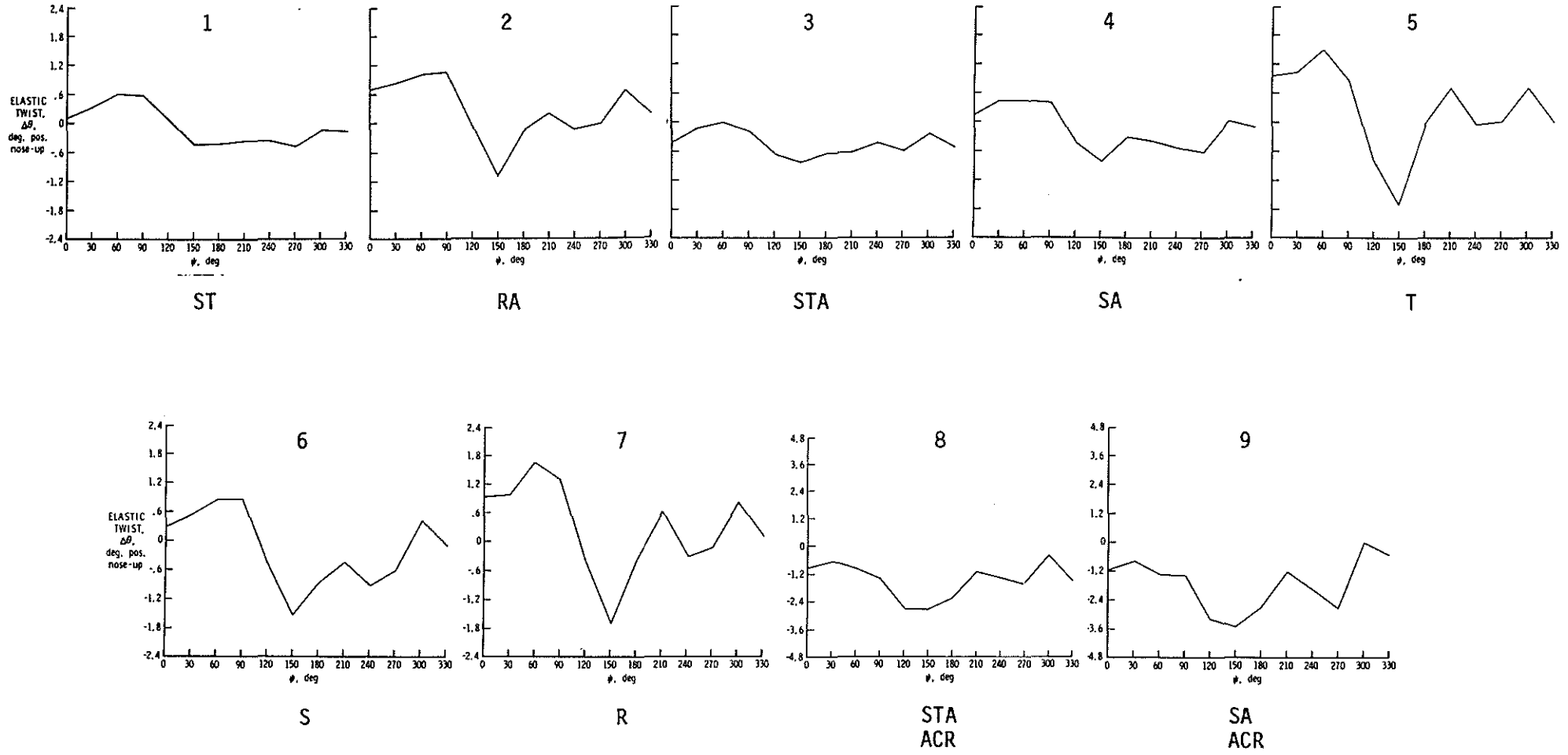

(b) $\mu = .35$ $M_T = .65$ $\frac{\overline{C}_L}{\sigma} = .07872$ $\alpha_s = -7.9°$. Performance rank at $C_D/\sigma = -.01250$

Figure 9.- Continued.

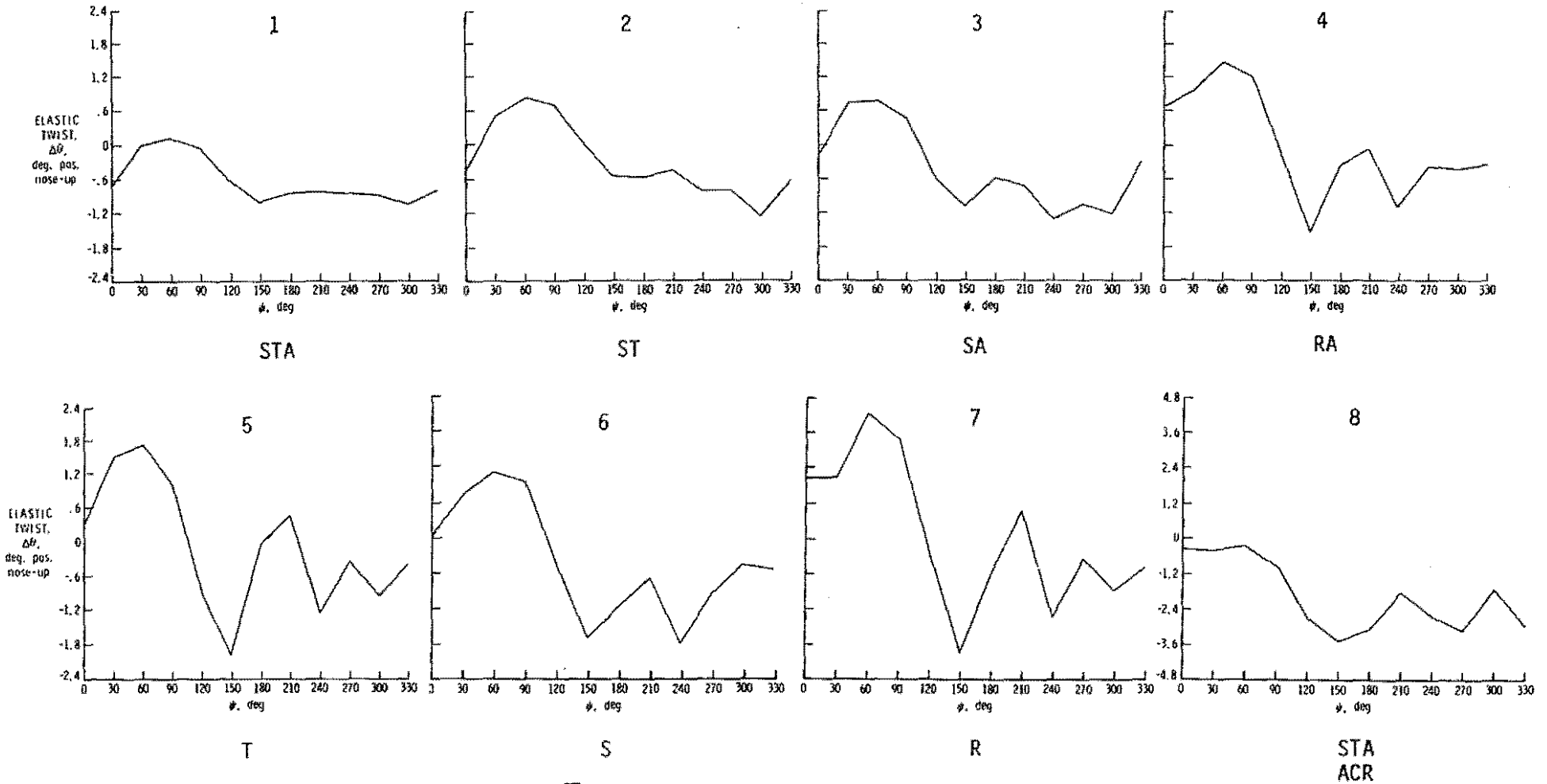

(c) $\mu = .35$ $M_T = .65$ $\frac{\overline{C_L}}{\sigma} = .098$ $\alpha_s = -4.9°$. Performance rank at $C_D/\sigma = -.0125$

Figure 9.- Continued.

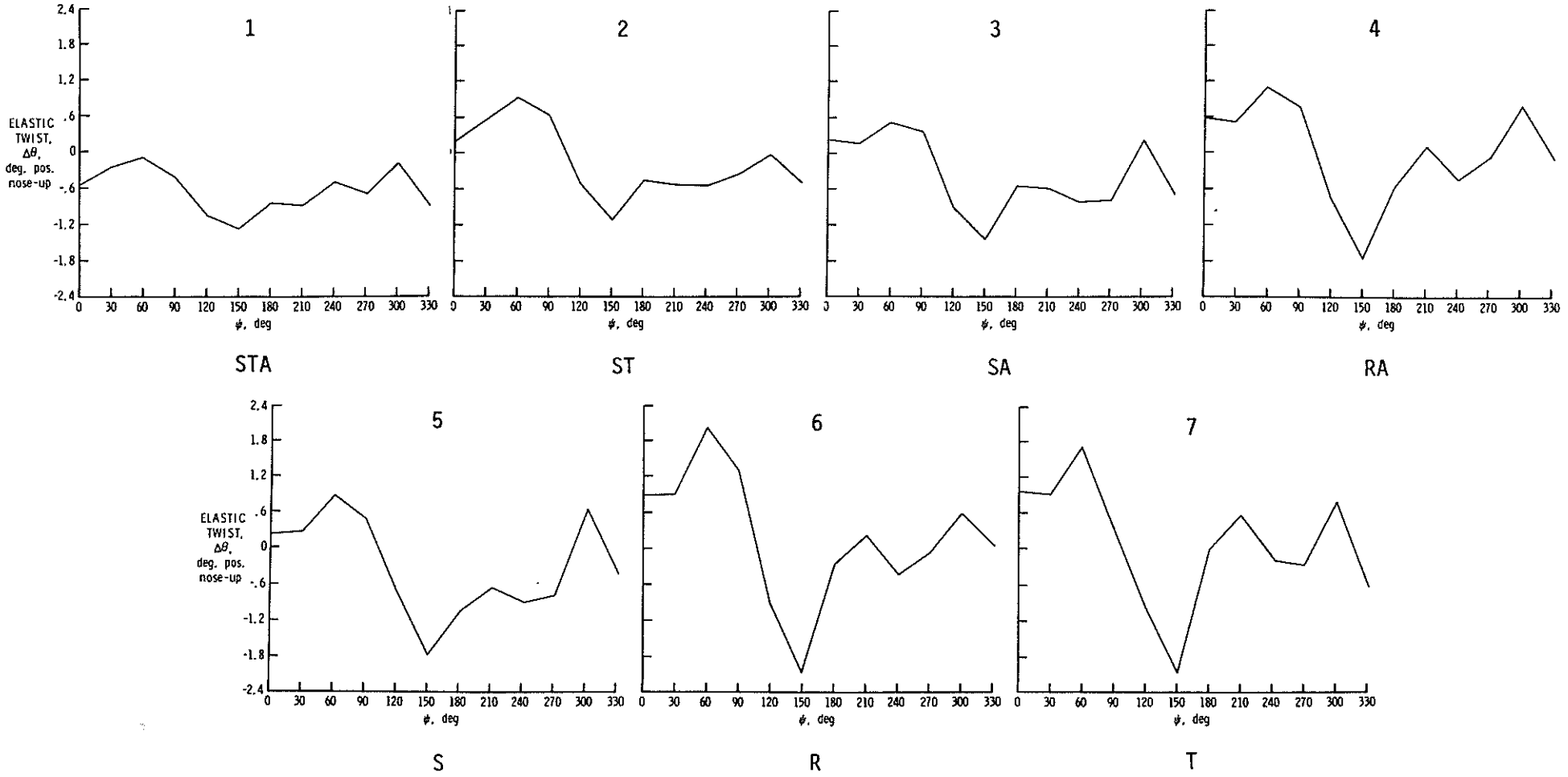

(d) $\mu = .40$ $M_T = .65$ $\frac{\overline{C_L}}{\sigma} = .07885$ $\alpha_s = -8.0°$. Performance rank at $C_D/\sigma = -.01350$

Figure 9.- Concluded.

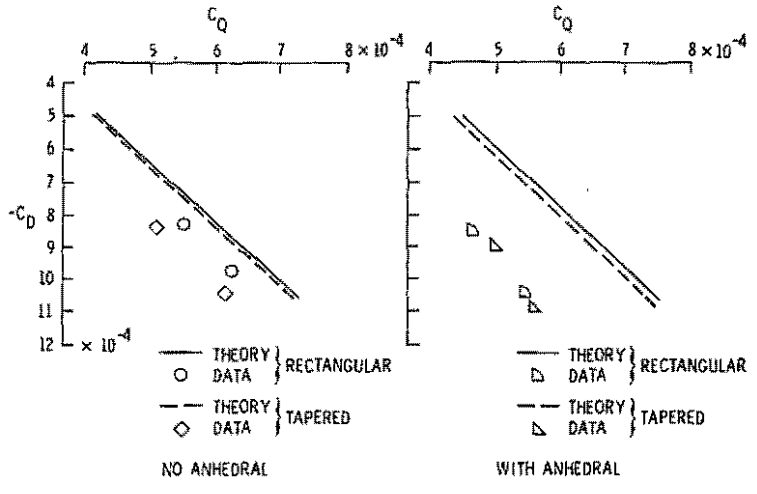

(a) Uniform inflow model

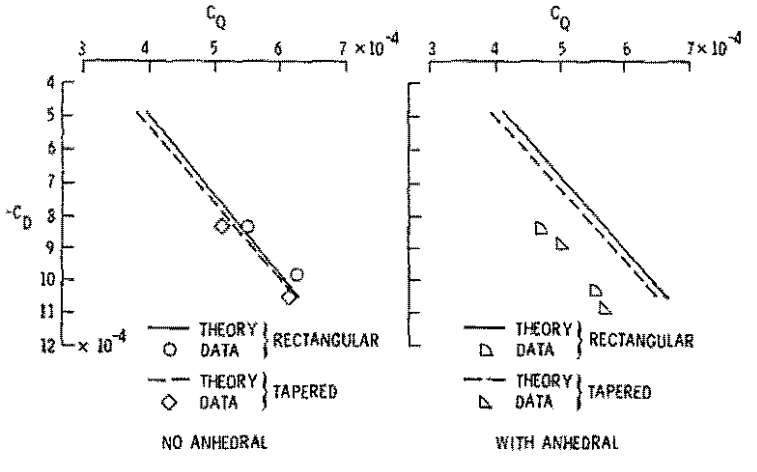

(b) Non-uniform inflow model

Figure 10.- Comparison of rotor performance with rigid blade analytical model $\mu = .35$, $\bar{C}_L/\sigma = .08$, $M_T = .65$.

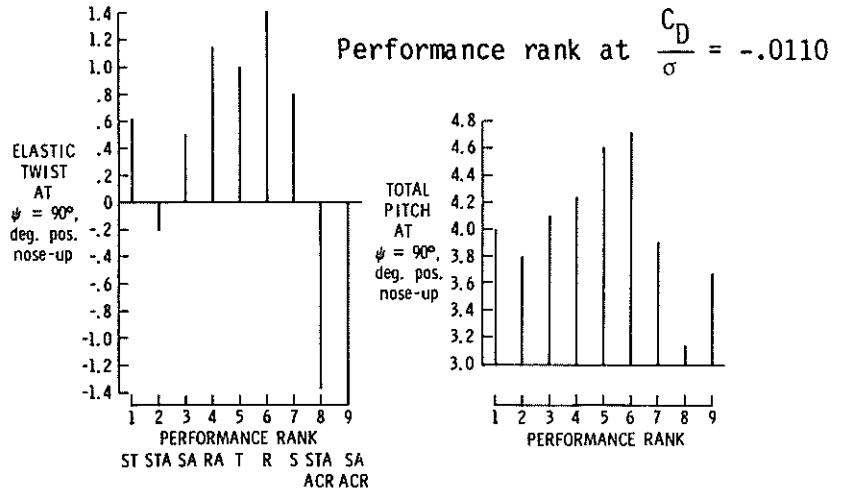

(a) μ = .35 $\frac{\overline{C}_L}{\sigma}$ = .07872 α_s = -6.1°

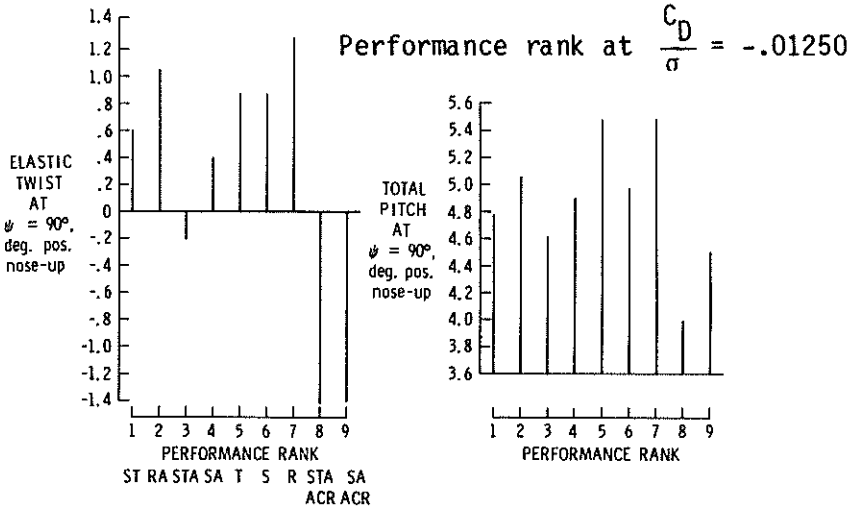

(b) μ = .35 $\frac{\overline{C}_L}{\sigma}$ = .07872 α_s = -7.9°

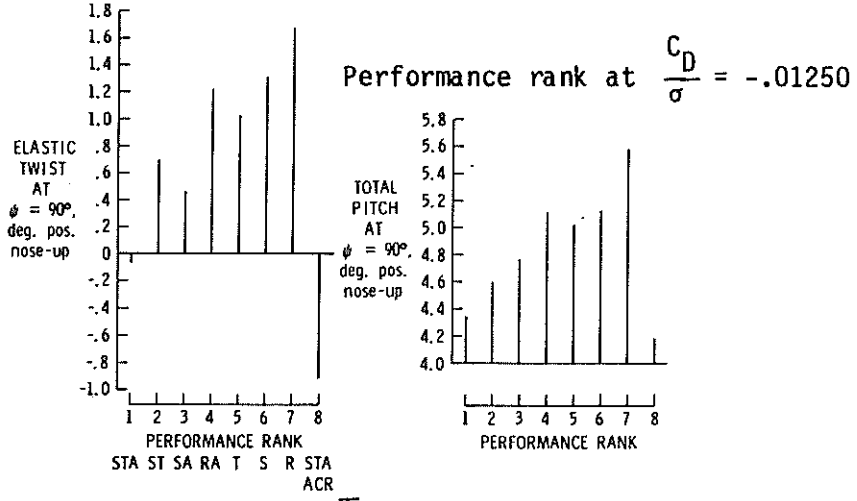

(c) μ = .35 $\frac{\overline{C}_L}{\sigma}$ = .098 α_s = -4.9°

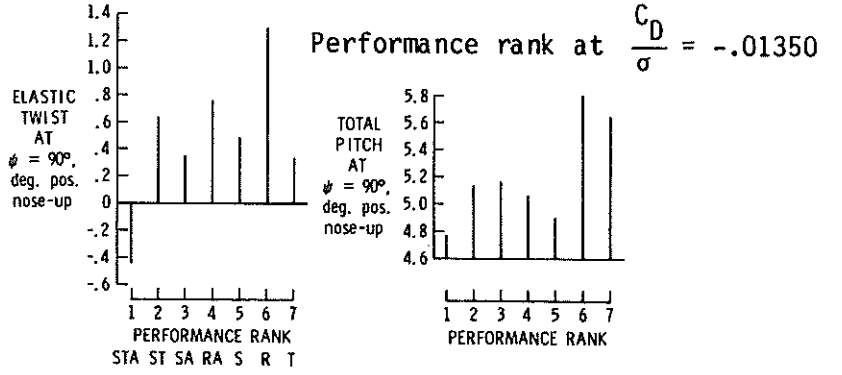

(d) μ = .40 $\frac{\overline{C}_L}{\sigma}$ = .07885 α_s = -8.0°

Figure 11.- Advancing side tip elastic twist and total pitch versus configuration performance (r/R = .78 M_T = .65).

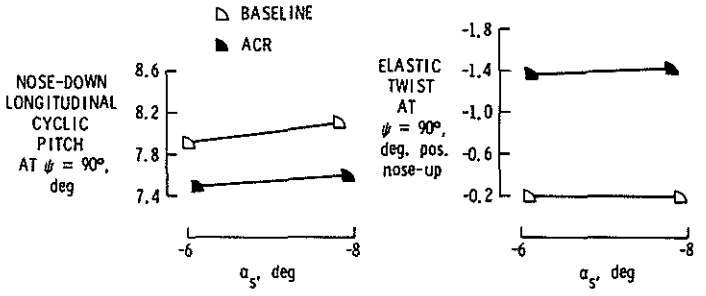

(a) Swept-Tapered Anhedral Tip

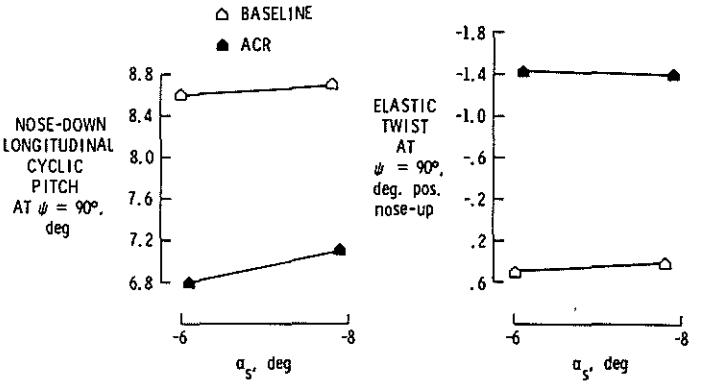

(b) Swept Anhedral Tip

Figure 12.- Advancing blade control angle and elastic twist versus α_S (μ = .35 M_T = .65 $\bar{C}_L/\sigma$ = .08).